

AN EFFICIENT STOCHASTIC BASED MODEL FOR SIMULATING MICROELECTRODE RECORDINGS OF THE DEEP BRAIN

Modelling and Analysis

K. J. Weegink¹, J. J. Varghese¹, P. A. Bellette¹, T. Coyne², P. A. Silburn³ and P. A. Meehan¹

¹*School of Mechanical and Mining Engineering, Faculty of Engineering, The University of Queensland,
4072, St Lucia, Australia*

²*St. Andrew's War Memorial Hospital, Brisbane, Australia*

³*Center for Clinical Research, The University of Queensland, 4029, Herston, Australia*

Keywords: Deep brain signals, Micro-electrode recordings, Point Process model.

Abstract: We have developed a computationally efficient stochastic model for simulating microelectrode recordings, including electronic noise and neuronal noise from the local field of 3000 neurons. From this we have shown that for a neuron network model spiking with a stationary Weibull distribution the power spectrum can change from exhibiting periodic behaviour to non-stationary behaviour as the distribution shape is changed. It is shown that the windowed power spectrum of the model follows an analytical result prediction in the range of 100-5000 Hz. The analysis of the simulation is compared to the analysis of real patient interoperative sub-thalamic nucleus microelectrode recordings. The model runs approximately 200 times faster compared to existing models that can reproduce power spectral behaviour. The results indicate that a spectrogram of the real patient recordings can exhibit non-stationary behaviour that can be re-created using this efficient model in real time.

1 INTRODUCTION

For the treatment of progressed movement disorders, such as Parkinson's disease (PD), deep brain stimulation (DBS) may be used. This treatment involves locating a target deep brain structure, such

as the sub-thalamic nucleus (STN), inserting an electrode to within 1 mm accuracy, and then applying a pulsed electric field to the area. One of the tools used to locate the correct nucleus structure is a microelectrode recording (MER). MERs are performed by inserting a recording electrode, with a

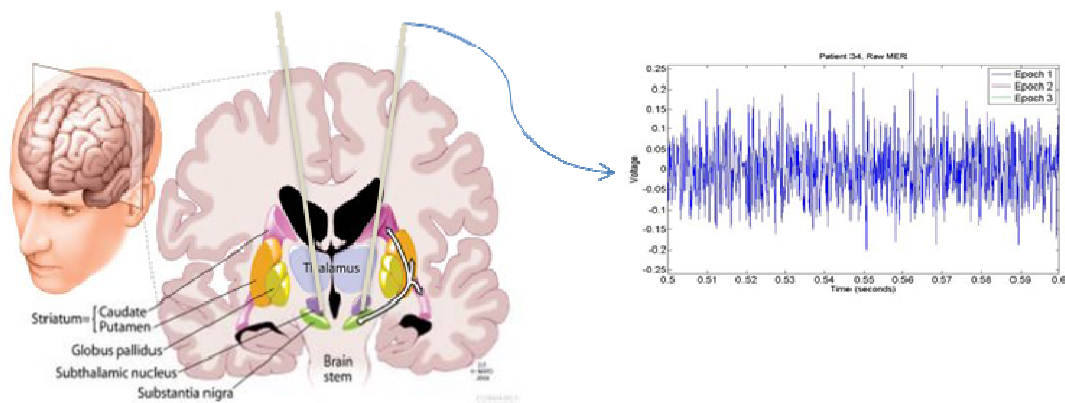


Figure 1: The micro-electrode recordings (MER) are acquired by inserting an electrode into a deep brain structure. The electrical activity of the neurons surrounding the electrode can couple to it producing a voltage time series.

diameter around 50 μm , into the nucleus structure (figure 1) located via MRI and CT scans.

To confirm the correct location of the implanted DBS electrodes, patients are awake to perform neurological tests. This gives an opportunity to monitor the candidate nucleus, for stimulation, while the patients perform tasks. Recent work has shown that with the correct measure, correlations between MER recordings and patient response to semantic tests has been demonstrated (P. A. Meehan & Bellette, 2009; Paul A. Meehan et al., 2011; Varghese et al., 2011).

Currently there has also been work on developing a bi-directional brain-machine interface for DBS treatment (Rouse et al., 2011). To further develop these research paths appropriate methods for efficient real time simulations to estimate neural network behaviour are required. For instance developing a metric that can characterise the underlying neural behaviour from a MER, a better understanding of the process in DBS could be made.

Current MER models only consider the behaviour of the closest neuron and reduce the further neurons to a local field noise (Santaniello, Fiengo, Glielmo, & Catapano, 2008). For feedback control of DBS the behaviour of the neural network needs to be modelled, as it has been shown that analysis of the closest neuron to the electrode is insufficient (Rouse, et al., 2011). Using the current non-linear neuron models of DBS (Rubin & Terman, 2004) for this type of feedback controller would be too computationally intensive, for this reason models that can take into account a large number of neurons and display markers of pathological states efficiently are needed.

In this paper we develop numerical probabilistic models, using a point process (PP) in order to create a much more computationally efficient model of networked neurons. Each neuron is coupled to the electrode, using a non-homogenous model for the extracellular medium, via a filter function derived from a conductance based model for the STN extracellular current during an action potential (AP). We use the model to compare with real patient MERs and an analytical model using frequency based analysis. This type of numerical model could potentially be used in a clinical setting as part of a feedback controller for DBS, alleviating the clinical load of optimizing the device settings.

2 METHODS

There are several aspects to modelling and analysing

deep brain signals. The system is a complicated system with many levels of dynamics required to create a MER. Section 2.1 contains the procedure used to acquire patient MERs. The factors that contribute to modelling a MER; modelling the behaviour of a single neuron, the network behaviour, the neuron electrode interaction and the electrical equipment processing the signal are detailed in the section 2.2. A simple analytical model is presented in 2.3 for comparison to the numerical model and to provide more insight into how the statistical distribution influences the expected power spectrum. The methods of the comparative analysis are then summarized in 2.4.

2.1 Experimental Procedure - Patient MER Acquisition

MERs are acquired from participants with idiopathic PD who were considered suitable for the implantation of bilateral permanent stimulators in the STN. Fused MRI and stereotactic CT images and direct visualisation of FLAIR (Fluid-attenuated inversion recovery) MRI images displayed by Stealthstation (Medtronic Inc., Minneapolis, MN) were used to target the STN.

During surgery characteristic STN firing patterns were used to confirm the STN location by the neurologist and neurosurgeon. More details of the surgical procedure are reported in Coyne et al. (Coyne et al., 2006).

MERs were acquired with a Tungsten microTargeting[®] electrode (model mTDWAR, FHC, Bowdoinham, ME) with a tip diameter of less than 50 μm and impedance of approximately 0.5 M Ω (\pm 30%) at 1 kHz. MERs were filtered (500-5000 Hz) and recorded at a sampling rate of 24 kHz from LeadPoint[™] (Medtronic Inc., Minneapolis, MN).

2.2 Numerical Modelling of Micro-Electrode Recordings

A MER is created by the activity of the neurons around the recording electrode. The neurons generate currents and hence electric fields that propagate through the different structures of the brain tissue, which can attenuate and filter the signal (Garonzik, Ohara, Hua, & Lenz, 2004). Finally the field incident on the electrode is processed by the electrical equipment to produce the recording.

Models of MERs have been developed that consider single unit recordings, made from a stochastic single neuron with random noise (Santaniello, et al., 2008) and local field potentials

(LFP) created using the spike trains of simultaneously recorded *in-vivo* cells (Bedard & Destexhe, 2009). However neither of these models allow for real time simulations with dynamically altering network behaviour.

To effectively model a MER which would allow real time simulations, there are several different stages that need to be taken into consideration. The four separate areas we are to model are the behaviour of the neural network, the electrical dynamics of individual neurons, the coupling of the electric fields from a neuron to the electrode and the processing of the signal by the electronics.

2.2.1 Neural Networks

For a MER a large number of neurons in the structure surrounding the electrode contribute to the signal. Dynamic models of neurons and neural networks are common for simulating brain structures (Feng, Shea-Brown, Greenwald, Kosut, & Rabinz, 2007; Izhikevich, 2007a, 2007b; Rubin & Terman, 2004; Terman, Rubin, Yew, & Wilson, 2002). These types of models, using synaptic connections between neurons with dynamical neuron models, can be very computationally intensive (Long & Fang, 2010). To reduce the computational burden of modelling individual neurons with synaptic connections, the firing times of each neuron can be characterized by a stochastic variable. This variable is produced from a probability distribution that depends upon the behaviour of the network. This type of model is a point process (Perkel, Gerstein, & Moore, 1967a, 1967b).

For single neurons the spiking statistics are often modelled by a Poisson distribution of inter spike interval (ISI) times. The participants for the deep brain MER recordings are undergoing treatment for a pathological state that is treated by altering STN function. This could imply abnormal function of the STN where the firing is not best described by a Poisson distribution in ISIs.

A probability distribution that can give the common types of behaviour found in neurons, such as bursting, Poisson and periodic behaviour, is the Weibull distribution (Li, 2011; McKeegan, 2002; Perkel, et al., 1967a, 1967b). This type of distribution can reduce to a Poisson distribution if the shape parameter is equal to one, takes the form of a Rayleigh distribution if the shape parameter is larger than two and burst fire behaviour is produced as it goes below one.

The point process simulation is performed using MATLAB 7.12.0 (R2011a) on a PC with a quad

core 1.73GHz processor and 8.0 GB of RAM. A spatial distribution of 3000 neurons is randomly generated, shown in figure 2, that follows the radial density of neurons ($N(r)$) given in equation (1) using a spatial neuron density of $\rho = 10^5 cm^{-3}$.

$$N(r) = 4\pi r^2 \rho. \quad (1)$$

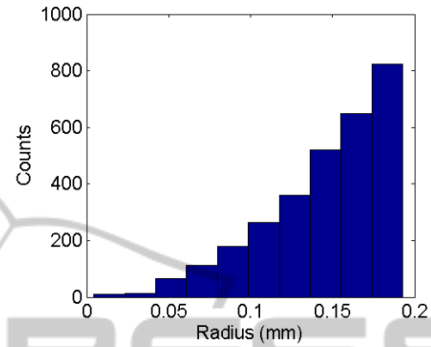


Figure 2: The radial distribution of neurons used for simulations. The volume of tissue for the simulation depends on the number of neurons simulated.

All simulations are performed over a three second period. Time series of Dirac pulses are created for each neuron by drawing interval times for spike occurrences from a probability distribution. Weibull distributions are used to generate the ISIs given by

$$P(t) = \begin{cases} \left(\frac{t-t_r}{\lambda}\right)^{c-1} \frac{c}{\lambda} e^{-\left(\frac{t-t_r}{\lambda}\right)^c} & x > t_r, \\ 0 & x \leq t_r \end{cases}, \quad (2)$$

λ is the scale parameter that controls the rate and is set to 10 Hz. The shape parameter c is varied to control the neuron behaviour; with $c \ll 1$ generating bursting, $c = 1$ Poissonian and $c \gg 1$ periodic behaviour. The parameter t_r controls the refractory time of the neuron and set to 5 ms, preventing another action potential occurring for the same neuron in this period. The first spike for each neuron uses $c = 1$ with $t_r=0$. Each time series is convolved with the EAP for an STN neuron by taking the product in the frequency domain. The time series data for each neuron are then superimposed to create the voltage at the electrode.

2.2.2 Neuron Dynamics

Using a PP model for the neural network, the dynamics of each neuron have been reduced to an 'on' or 'off' state. To develop the correct response for a neuron when in the 'on' state, conductance models such as the Hodgkin and Huxley (HH) model can be used to generate the behaviour of the

individual neuron, when an action potential occurs.

The HH model can calculate the extracellular currents around a neuron which is required for determining the voltage seen by an electrode. It has previously been demonstrated STN cells can be simulated effectively using this type of model (Terman, et al., 2002). More computationally efficient mathematical models of neurons are not considered since these types of models cannot always reproduce the correct shape of the action potential waveform, and this feature is important when considering the windowed power spectrum.

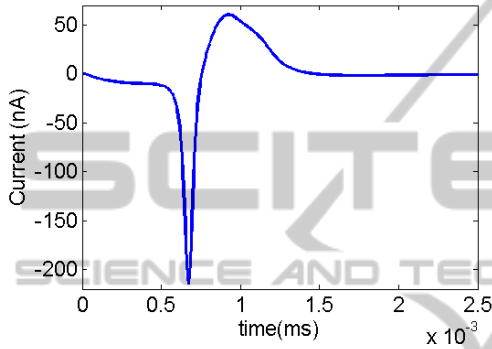


Figure 3: The extracellular current used for each neuron generated using equation (3).

The STN cell is modelled using a single compartment conductance based model described by a modified version of the HH equation, based on (Feng, et al., 2007; Rubin & Terman, 2004; Terman, et al., 2002):

$$C_m \frac{dv}{dt} = -g_L(V - v_L) - g_K n^4 (V - v_K) - g_{Na} m^3 h (V - v_{Na}) - g_T a^3 b^2 (V - v_{Ca}) - g_{Ca} s^2 (V - v_{Ca}), \quad (3)$$

where C_m is the membrane capacitance and set to $1 \text{ pF}/\mu\text{m}$; g_L, v_L are the leak conductance and reversal potential ($2.25 \text{ nS}/\text{m}^2$ and -60.0 mV respectively); g_K, v_K are the K^+ conductance and equilibrium potential ($45 \text{ nS}/\text{m}^2$ and -80.0 mV respectively); g_{Na}, v_{Na} are the Na^+ conductance and equilibrium potential ($37.5 \text{ nS}/\text{m}^2$ and 55.0 mV respectively); g_T is a low-threshold T-type Ca^{2+} conductance ($0.5 \text{ nS}/\text{m}^2$); and g_{Ca}, v_{Ca} are a high-threshold Ca^{2+} conductance and a Ca^{2+} equilibrium potential ($0.5 \text{ nS}/\text{m}^2$ and 140.0 mV respectively). The gating variables n, m, h, a and b follow the differential equations given in (Terman, et al., 2002) using the parameters given in their table 1. The dynamics of a single neuron are modelled in NEURON (Hines & Carnevale, 1997) using equation (3) to generate the extracellular current

during an action potential, shown in figure 3.

2.2.3 Neuron/Electrode Interaction

The electrode senses the neuron dynamics through the electric field that propagates from the neuron. This electric field is known as the extracellular action potential (EAP). The EAP is generated by ionic currents around the active neuron. As the EAP propagates through the extracellular space to the electrode it will pass through regions of space with different conductivity and permittivity. This will cause filtering effects along with attenuation of the field. This means that the electrode will record a different EAP for each neuron depending upon the distance from the electrode and the media in between.

The complex impedance ($Z_\omega(r)$) for the interaction of each neuron with the electrode over the range of radii is calculated by (Bedard, Kroger, & Destexhe, 2004),

$$Z_\omega(r) = \frac{1}{4\pi\sigma(R)} \int_r^\infty \frac{1}{r'^2} \frac{\sigma(R) + i\omega\epsilon(R)}{\sigma(r') + i\omega\epsilon(r')} dr', \quad (4)$$

where σ is the conductivity in the extracellular medium, ϵ is the permittivity in the extracellular medium and R is the spherical radial size of each neuron. An exponentially decaying conductance

$$\sigma(r) = \sigma(R) \left(\sigma_0 + (1 - \sigma_0) e^{-\frac{r-R}{\lambda}} \right), \quad (5)$$

with a space constant $\lambda = 500 \mu\text{m}$, cell radius $R = 10 \mu\text{m}$, conductivity at the cell $\sigma(R) = 1.5 \text{ S}/\text{m}$ and a normalized low amplitude conductivity $\sigma_0 = 2 \times 10^{-9}$; and a constant normalized permittivity $\epsilon = 10^{-11} \text{ F}/\text{m}$ were used following Bedard (2004). The EAP waveform in the frequency domain for each neuron is calculated using the complex impedance and the FFT of the extracellular current.

The voltage (V_ω), in terms of the frequency components, at the electrode caused by a neuron is then calculated using Ohm's law (Bedard, et al., 2004),

$$V_\omega(r) = I_\omega Z_\omega(r), \quad (6)$$

where I_ω is the frequency component of the current at the neuron.

2.2.4 Electrical Processing

To properly analyse a MER the effects of the electrical equipment, on the recording, need to be included. These effects include the introduction of noise, such as that due to sampling rate, clock

stability and thermal noise, and any filtering that occurs. These issues could greatly affect the ability of a measure to differentiate the neuronal behaviour from the electrical effects.

The first such noise source is the noise present from thermal fluctuation of electrons in the microelectrode (Akingba, Wang, Chen, Neves, & Montemago, 2003). This type of noise is known as Johnson-Nyquist noise and is characterized by having zero mean voltage and a variance dependant on the temperature, resistance and frequency bandwidth.

The phase noise is not considered in this analysis due to the stability of the 10 MHz clock typically used and the comparatively small sample rate of 24 kHz. Digitization noise can be accounted for by producing the final MER of the simulation with the same time step that the patient data is recorded at. Finally any filters can be added using the filter transfer function in the post processing of the MER simulation.

Thermal noise on the electrode is added as white noise using

$$\langle V \rangle = 0, \quad (7)$$

$$\langle V^2 \rangle = 4k_B TR \Delta f, \quad (8)$$

where k_B is Boltzmann's constant, T is the temperature, R is the resistance, Δf is the bandwidth and $\langle \ \rangle$ is the time average, it is found that for a 0.5 M Ω resistor at body temperature (37°C) the thermal noise can be between 10-30% of the size of the neural signal.

The recording is filtered with a 6th order low pass Butterworth filter with a corner frequency of 5 kHz and a 3rd order high pass filter with a corner frequency of 500 Hz. The final MER from the simulation is produced with a sample rate of 24 kHz to create the same digitization effects as present in the patient data.

2.3 Simplified Analytical Model of Micro-Electrode Recordings

The MER may be analytically modelled by a superposition of independent spike trains, equivalent to the numerical model using a point process. The PSD for a PP model will be a filtered version of the PSD for the EAP waveform. For independent overlapping pulse trains, with the same shape waveform for each pulse, it has been shown (Banta, 1964) that the power spectrum ($G_0(\omega)$) for the MER can be written as

$$G_0(\omega) = \frac{vG(\omega)}{2\pi} \left[\overline{a^2} - 2\overline{a^2} \operatorname{Re} \left\{ \frac{H(\omega)}{1-H(\omega)} \right\} \right], \quad (9)$$

where $G(\omega)$ is the PSD of the waveform, $H(\omega)$ is the characteristic function (Fourier transform) of the probability distribution for the aggregate spiking statistics, v is the number of pulses per unit time and a is the amplitude of the pulses with $\overline{\ \ }$ representing the ensemble average.

Although this equation for the PSD takes into account the attenuation caused by the extracellular medium on the spike waveform it does not take into account the frequency filtering effects.

This equation can however be used to see expected behaviour of different simulations. The bracketed term can be thought of as a filter, which is a function of the spiking probability, applied to the waveform PSD. By looking at this term the filtering effects caused by the different probability functions can be examined.

2.4 Procedure for Comparison of Numerical and Experimental Results

The most intuitive way to analyse the noise of an MER is to look at the PSD. This was first done by in 1979 (McNames, 2004) using a circuit equivalent of a Fourier Transform (FT). In recent years analysis of MERs has progressed into the digital domain. The majority of these techniques still involve analysis of the PSD.

Neuron spiking behaviour can be examined through MER PSDs. It was shown how f^{-2} behaviour in the PSD can arise from shot noise type behaviour of neurons spiking (Milstein, Mormann, Fried, & Koch, 2009), while f^{-1} behaviour may be due to filtering by reactive extracellular media, or due to complex self-organized critical phenomena (Bedard & Destexhe, 2009).

Complex measures have been used to look at MERs, and it has been shown that some techniques, such as the Non-Markov parameter (NMP) relate to the PSD (Varghese, et al., 2011).

The windowed PSD will not capture transient behaviour in the MER. To view this transient behaviour a spectrogram can be used. This involves dividing the signal into smaller time bins. The PSD is taken for each time bin to see the PSD as a function of time for the MER.

A windowed PSD is taken of the time series data from the simulation using a Gaussian window with an e^{-2} width of 1/50th of the signal length. The PSD is then averaged of 5 trials of the simulation with the same firing statistics. This is compared to the windowed PSD of a three second signal averaged over 5 recordings.

Spectrograms are produced with the same time intervals used for the windowed PSD. The spectrograms consist of a series of instantaneous PSD over each time interval. The spectrograms are then used to compare the stationary behaviour of the power spectrum for different ISI probability distributions and the patient data.

3 RESULTS AND DISCUSSION

The results from the numerical simulations are presented in this section and are then compared to the experimental results and analytical predictions. Subsection 3.1 summarises the numerical results and provides a comparison with MERs acquired from patients. The time series, windowed power spectrum and spectrogram for three different simulation parameters are used. Subsection 3.2 includes details of the results from the simple analytical model, comparing how the power spectrum of the EAP is modified under the different spiking statistics used to produce the MERs from the numerical models.

3.1 Numerical and Experimental Results Comparison

The time series of voltage from the simulations has been plotted for three different firing probability distributions and compared to a patient recording (Figure 4). For $c \cong 1$ the time series have similar features to the patient data. Differences can only be seen for large deviations from $c = 1$. As case examples for their characteristic behaviour extreme cases of c have been used. As $c \ll 1$, bursting behaviour is visible in the time series and for $c \gg 1$ periodic spiking becomes apparent.

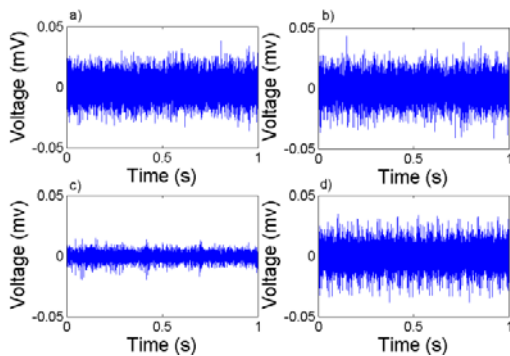


Figure 4: Comparison of a) Patient MER to simulations with b) $c = 1$, c) $c \ll 1$ and d) $c \gg 1$.

The simulations were calculated at a rate of 6 milli seconds per neuron per second of computational time, a 200 fold increase on dynamical models that reproduce accurate waveform shapes (Long & Fang, 2010).

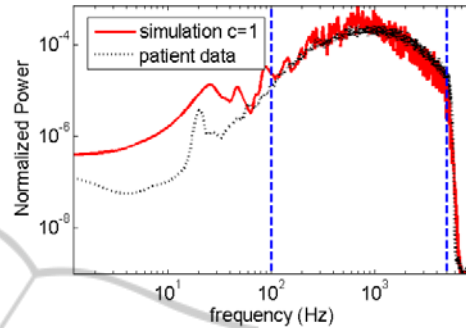


Figure 5: Overlap of the real patient windowed PSD over the windowed PSD of the simulation for $c = 1$.

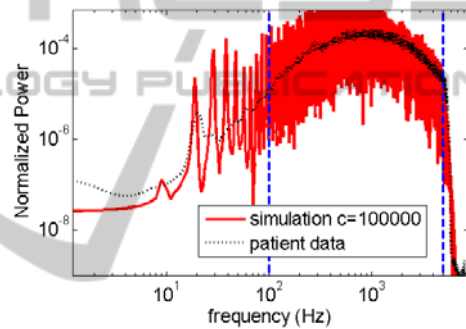


Figure 6: Overlap of the real patient windowed PSD over the windowed PSD of the simulation for $c \gg 1$.

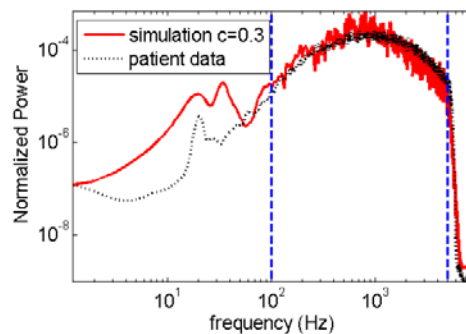


Figure 7: Overlap of the real patient windowed PSD over the windowed PSD of the simulation for $c \ll 1$.

The windowed PSD for all three simulations and the patient recordings, seen in figures 5, 6 & 7, have three main regions. The first region is the filter drop off above 5 kHz. This feature is present in all 4 PSDs with good agreement between patient data and simulations. The thermal noise term added is white

noise and as such adds the same power to every frequency, shifting the PSD up. This effect is removed by normalizing the power spectrum to integrate to unity. The other electrical effects; high and low pass filtering; do however alter the normalized power spectrum, seen by the sharp falloff in power in this region.

The second region is the behaviour at high frequencies (100-5000 Hz). The two simulations with $c \leq 1$ have good agreement with patient data in this region shown in figures 5 & 7. The simulation with $c \gg 1$ (figure 6) has structure in this region that can be explained as harmonics of features in the low frequency region. The overall shape in this region is dominated by the waveform of the EAP.

The final region of interest is in the region below 100 Hz. This region is thought to contain information of the Local field potential (LFP). Experimentally this region has an electronic filter, with a slow drop off. For $c \gg 1$ this region has a sharp peak at 10 Hz, the simulated spike rate, and then has peaks at the harmonic frequencies of $n \cdot 10$ Hz, where n is an integer. The other two cases have anomalous peaks in this region similar to the 20 Hz peak in the patient data. This beta band peak (12-30 Hz) has been seen in PD MER recordings previously and has been implicated in the pathological state (Eusebio & Brown, 2009).

Besides the PSD for $c \gg 1$, the problem with comparing the average PSD is that they appear very similar between 100-5000 Hz with differences below 100 Hz. Another method to examine the spectral properties of an MER is to look at the

spectrogram, figure 8, and to observe changes in the power spectrum over time.

From the spectrogram for the typical patient MER recording it can be seen that the PSD changes in time. These recordings show the feature in the beta band appearing and disappearing through the recording.

When the numerical simulations were performed with $c \gg 1$, the PSD appears periodic stationary. This behaviour can be seen in figure 8 d). When c is set to one or below features of the PSD appears to change in time in the beta band. This is similar behaviour to the PSD for the patient data.

This analysis suggests that $c \cong 1$ qualitatively represents the patient data the best from the options tried. This supports the idea that spiking behaviour in a large network appears Poisson (Câteau & Reyes, 2006; McNames, 2004; Stevens & Zador, 1998).

3.2 Analytical Predictions

The results from equation (5) show the effect of changes in the aggregate probability distribution. Equation (5) can be thought of as a spike waveform filter that is dependent on the probability distribution through $Re[H(\omega)/(1-H(\omega))]$. Figure 9 shows the frequency behaviour of equation (5) for different values of c , if the statistics follow a Weibull distribution.

For $c \gg 1$ and $c = 1$ figure 9 shows the frequency filtering effects due to the spiking statistics are flat and will not add noticeable features in the PSD below 100 Hz. This analytical model doesn't take into account the frequency filtering of

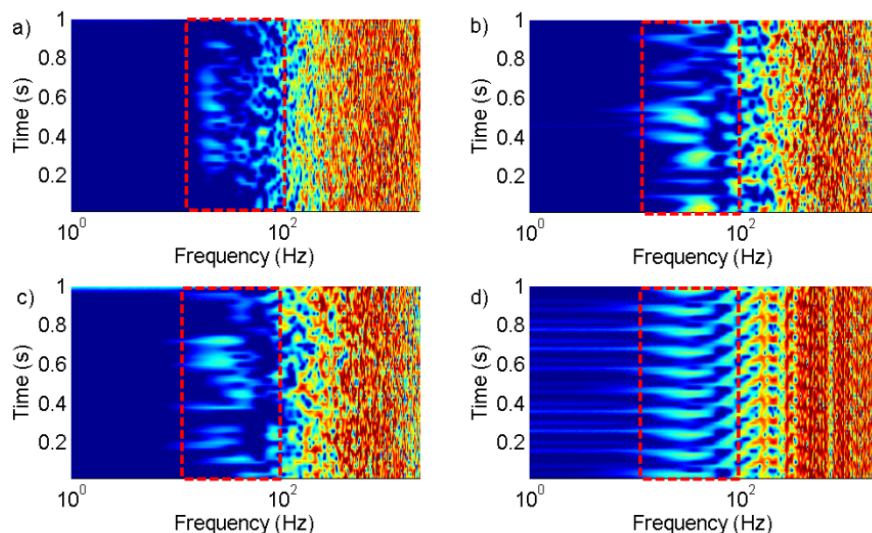


Figure 8: Spectrograms with the region displaying beta band behaviour boxed in red, a) patient MER showing transient beta band behaviour, b) simulations $c \ll 1$ showing transient beta band behaviour, c) $c = 1$ showing transient beta band behaviour and d) $c \gg 1$ showing periodic behaviour.

more distant neurons by the extracellular medium. Figure 9 a) shows how the extracellular medium model acts as a low pass filter. For these reasons this model is not sufficient to describe the features seen in the numerical simulations below 100 Hz.

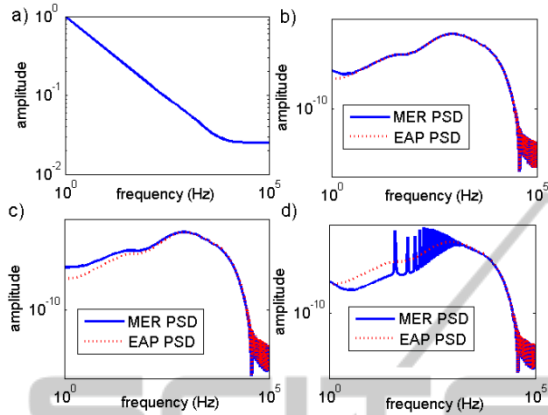


Figure 9: a) The filter function of the extracellular medium at $0.2\mu\text{m}$. Inserts b)-d) show the comparison of the power spectrum of the EAP with the MER power spectrum from the analytical model, b) the MER PSD for $c = 1$ modelled by equation (9), it can be seen that for this distribution the results of the MER and EAP PSDs are in agreement, c) the MER PSD for $c \gg 1$ modelled by equation (9), d) the MER PSD $c \ll 1$ modelled by equation (9).

For $c \gg 1$ the 10 Hz peak with harmonic peaks in the numerical simulation can be seen in the frequency effects from equation (9), shown in figure 9, if the aggregate probability distribution maintains the single neuron ISI probability shape.

The problem with this analysis is that we have assumed that the distribution controlling the ISIs is stationary in time. Equation (9) cannot account for ISI distributions that change in time. The non-stationary nature of the real patient PSD could suggest that the probability distribution describing the neuron firing may not be stationary. This behaviour can alternatively be explained by the probabilistic nature of the simulation and the time period the PSD is taken over. This is demonstrated by the simulations using the PP model showing similar non stationary behaviour under the same analysis, even though the probability distribution of ISIs was stationary in time.

4 CONCLUSIONS

MERs were efficiently simulated using a PP model with a conductance model for generating the EAP, taking into account extracellular frequency filtering

and attenuation; and the effects of the recording electronics. The simulations perform approximately 200 times faster than using a Hodgkin and Huxley model for all of the neuron dynamics (Long & Fang, 2010). With this computationally efficient model very good agreement was achieved when comparing the windowed PSD of the simulated MERs with real patient data for frequencies above 100 Hz.

Below 100 Hz the PSD of patient MERs are not stationary, which can be reproduced using a time stationary probability distribution for the ISI. Since the model is a probabilistic model that treats the neurons as point sources rather than a full dynamical model, the neurons are either in an 'on' or 'off' state. This means it cannot produce neural features such as sub-threshold oscillations and cellular activity such as synaptic currents. These features may be critical for describing the features below 100Hz sufficiently.

The analytical model using the results from Banta (1964) showed features that were present in the simulations, such as the harmonic structure present in the windowed PSD for simulations with $c \gg 1$. This type of analysis could allow for characterization of the ISI probabilities of patient MERs from the windowed PSD.

To account for the features in the beta band (10-35 Hz) more complex models; including explicit network interactions and full cell dynamics, such as sub-threshold oscillations, may be required.

Future work could include performing the inverse problem of finding the shape and rate parameters that best describe a patient MER. The results from this study could be used to find markers that may be applicable in the clinical environment for optimising DBS and potentially operating in a feedback controller.

ACKNOWLEDGEMENTS

The authors are greatly indebted to PD specialists of St. Andrew's War Memorial and The Wesley Hospitals, Australia for their motivation, guidance, interdisciplinary expertise and funding.

REFERENCES

- Akingba, A. G., Wang, D., Chen, P.-s., Neves, H., & Montemago, C. (2003). *Application of nanoelectrodes in recording biopotentials*. Paper presented at the IEEE-NANO 2003.

- Banta, E. (1964). A note on the correlation function of nonindependent, overlapping pulse trains. *Information Theory, IEEE Transactions on*, 10(2), 160-161.
- Bedard, C., & Destexhe, A. (2009). Macroscopic Models of Local Field Potentials and the Apparent 1/f Noise in Brain Activity. *Biophysical Journal*, 96, 2589-2603.
- Bedard, C., Kroger, H., & Destexhe, A. (2004). Modeling Extracellular Field Potentials and the Frequency-Filtering Properties of Extracellular Space. *Biophysical Journal*, 86, 1829-1842.
- Câteau, H., & Reyes, A. D. (2006). Relation between Single Neuron and Population Spiking Statistics and Effects on Network Activity. *Physical Review Letters*, 96(5), 058101.
- Coyne, T., Silburn, P. A., Cook, R., Silberstein, P., Mellick, G., Sinclair, F., & Stowell, P. (2006). Rapid subthalamic nucleus deep brain stimulation lead placement utilising CT/MRI fusion, microelectrode recording and test stimulation. *Acta Neurochirurgica Suppl*(99), 49-50.
- Eusebio, A., & Brown, P. (2009). Synchronisation in the beta frequency-band—the bad boy of parkinsonism or an innocent bystander? *Experimental Neurology*, 217(1), 1-3.
- Feng, X.-J., Shea-Brown, E., Greenwald, B., Kosut, R., & Rabitz, H. (2007). Optimal deep brain stimulation of the subthalamic nucleus—a computational study. *J. Comput. Neurosci.*(23), 265–282.
- Garonzik, I. M., Ohara, S., Hua, S. E., & Lenz, F. A. (2004). Microelectrode Techniques: Single-Cell and Field Potential Recordings. In Z. Israel & K. J. Burchiel (Eds.), *Microelectrode recordings in movement disorder surgery* (Vol. 1). New York: Thieme Medical Publishers, Inc.
- Hines, M. L., & Carnevale, N. T. (1997). The NEURON Simulation Environment. *Neural Computation*, 9(6), 1179-1209. doi: 10.1162/neco.1997.9.6.1179
- Izhikevich, E. M. (2007a). *Dynamical Systems in Neuroscience*. Cambridge: MIT Press.
- Izhikevich, E. M. (2007b). Solving the distal reward problem through linkage of STDP and dopamine signaling. *Cerebral Cortex*, October(17), 2443-2452.
- Li, C. (2011). A Model of Neuronal Intrinsic Plasticity. *Autonomous Mental Development, IEEE Transactions on*, PP(99), 1-1.
- Long, L. N., & Fang, G. (2010). *A Review of Biologically Plausible Neuron Models for Spiking Neural Networks*. Paper presented at the AIAA InfoTech@Aerospace Conference, Atlanta, GA.
- McKeegan, D. E. F. (2002). Spontaneous and odour evoked activity in single avian olfactory bulb neurones. *Brain Research*, 929(1), 48-58. doi: 10.1016/s0006-8993(01)03376-5
- McNames, J. (2004). Microelectrode Signal Analysis Techniques for Improved Localization. In Z. Israel & K. J. Burchiel (Eds.), *Microelectrode recordings in movement disorder surgery* (Vol. 1). New York: Thieme Medical Publishers, Inc.
- Meehan, P. A., & Bellette, P. A. (2009). *Chaotic Signal Analysis of Parkinson's Disease STN Brain Signals*. Paper presented at the Topics in Chaotic Systems.
- Meehan, P. A., Bellette, P. A., Bradley, A. P., Castner, J. E., Chenery, H. J., Copland, D. A., & Silburn, P. A. (2011). *Investigation of the Non-Markovity Spectrum as a Cognitive Processing Measure of Deep Brain Microelectrode Recordings*. Paper presented at the BIOSIGNALS 2011- International Conference on Bio-Inspired Systems and Signal Processing, Rome, Italy.
- Milstein, J., Mormann, F., Fried, I., & Koch, C. (2009). Neuronal Shot Noise and Brownian 1/f² Behavior in the Local Field Potential. *PLoS One*, 4(2), e4338 4331-4335.
- Perkel, D. H., Gerstein, G. L., & Moore, G. P. (1967a). Neuronal Spike Trains and Stochastic Point Processes I. *Biophys J.*, 7(4), 391–418.
- Perkel, D. H., Gerstein, G. L., & Moore, G. P. (1967b). Neuronal Spike Trains and Stochastic Point Processes II. *Biophys J.*, 7(4), 419–440.
- Rouse, A. G., Stanslaski, S. R., Cong, P., Jensen, R. M., Afshar, P., Ullestad, D., & Denison, T. J. (2011). A Chronic Generalized Bi-directional Brain-Machine Interface. *J. Neural Eng.*, 8(036018).
- Rubin, J. E., & Terman, D. (2004). High Frequency Stimulation of the Subthalamic Nucleus Eliminates Pathological Thalamic Rhythmicity in a Computational Model. *Journal of Computational Neuroscience*(16), 211–235.
- Santaniello, S., Fiengo, G., Glielmo, L., & Catapano, G. (2008). A biophysically inspired microelectrode recording-based model for the subthalamic nucleus activity in Parkinson's disease. *Biomedical Signal Processing and Control*(3), 203–211.
- Stevens, C. F., & Zador, A. M. (1998). Input synchrony and the irregular firing of cortical neurons. *Nature Neuroscience* 1, 210 - 217. doi: 10.1038/659
- Terman, D., Rubin, J. E., Yew, A. C., & Wilson, C. J. (2002). Activity Patterns in a Model for the Subthalamopallidal Network of the Basal Ganglia. *The Journal of Neuroscience*, 7(22), 2963–2976.
- Varghese, J. J., Weegink, K. J., Bellette, P. A., Meehan, P. A., Coyne, T., & Silburn, P. A. (2011). *Theoretical & Experimental Analysis of the Non Markov Parameter to Detect Low Frequency Synchronisation in Time Series Analysis*. Paper presented at the Engineering in Medicine and Biology Society, Annual International Conference of the IEEE, Boston Massachusetts.